



# Pitting Corrosion Behavior of F304 Stainless Steel Under the Exposure of Ferric Chloride Solution

Surinder Pal<sup>1</sup> · Shailendra Singh Bhadauria<sup>1,2</sup> · Pramod Kumar<sup>2</sup>

Received: 19 June 2019 / Revised: 14 August 2019 / Accepted: 27 August 2019 / Published online: 9 September 2019  
© Springer Nature Switzerland AG 2019

## Abstract

Present paper deals with an experimental investigation of pitting corrosion of forged 304 stainless steel. Material is exposed to ferric chloride solution to investigate the effect of pitting corrosion. This material is known to provide structural strength with improved toughness and ductility. A number of experiments were carried out on F304 SS under ferric chloride solution by putting it for three different time durations of 8 h, 16 h, and 24 h. The results specify that pit formation increases over time. During experimentation, the number of pits, pit depth, corrosion rate, weight loss, and average pit depth have been measured. Microstructural characterization and surface roughness tests were carried out on the chemically exposed surface to understand the growth of pitting corrosion. Fractographic images high-end microscopy showed that the ferric chloride solution initiates the pitting of 304 austenite stainless steel. Furthermore, the exposure leads to the formation of a number of small pits that coalesce together to form cracks that appear at the bottom of the pit. It was also confirmed that the appearance of small bottom pits initiates cracks by increasing the duration of corrosion test to 24 h which is only due to dissolved inclusive atoms of chloride as revealed by EDX analysis.

**Keywords** F304 stainless steel · Pitting corrosion · Corrosion rate · Pit depth · Ferric chloride solution

## 1 Introduction

Austenite stainless steel is widely used for the corrosive environment. Present work is focused on understanding the effect of ferric chloride solution on F304 stainless steel which is widely used for various industrial applications (such as petroleum, food, medicine, and other industries). The purpose of this study is to examine the corrosive behavior of the material and to observe its effect with respect to time. Many researchers have studied corrosion susceptibility of 304 stainless steel under different chemical solutions

with varying pH and temperatures. Vogiatzis et al. examined the corrosion behavior of 304 austenitic stainless steel in simulated oil field produced water at 25 °C, and their results indicated that the corrosion rate is reduced with time [1]. Street et al. analyzed the atmospheric pitting corrosion of material 304 L stainless steel by using droplets of MgCl<sub>2</sub> for 24 h at temperature 30 °C. It was revealed that the pit morphology was a sensitive function of relative humidity (RH) [2, 3]. Degerbec et al. tested the specimens of steel type 18Cr–2Mo–Ti which were exposed for 1, 3, and 5 years in a marine atmosphere. It was observed that in a near-coastal area, the stainless steel type 18Cr–2Mo–Ti is well suitable for usage in building applications [4, 5]. Xie et al. determined the change in pitting corrosion from the statistics of pitting during the test duration up to 720 h exposed to highly concentrated chloride solutions. It revealed that the resistance to pitting corrosion was considerably affected by chloride concentration and temperature. [6]. Prosek et al. studied the application limits of different austenitic and austenitic–ferritic (duplex) stainless steels subjected to tensile stress. Furthermore, the corrosivity of chloride deposits under given exposure conditions decreased in the following order: calcium chloride (CaCl<sub>2</sub>) > magnesium

---

✉ Surinder Pal  
Surinder92.pal@gmail.com  
Shailendra Singh Bhadauria  
bhadauriass@nitj.ac.in  
Pramod Kumar  
kushwahapramod@nitj.ac.in

<sup>1</sup> Department of Industrial and Production Engineering, Dr. B R Ambedkar National Institute of Technology Jalandhar, Jalandhar, Punjab 144011, India

<sup>2</sup> Dr. B R Ambedkar, National Institute of Technology Jalandhar, Jalandhar, Punjab 144011, India

chloride ( $\text{MgCl}_2$ ) > sodium chloride ( $\text{NaCl}$ ) [7]. Prosek et al. investigated the corrosion performance of austenitic and austenitic–ferritic (duplex) stainless steels in the existence of chloride deposits simulating non-rinsing atmospheric environments. It was reported that in the presence of calcium chloride solution, the stress corrosion cracking (SCC) was susceptible even at low temperatures (20 °C and 30 °C) particularly in the cases of 304 L and 316 L stainless steels [8]. Typically, the pitting initiates at the surface active sites, such as inclusion and chromium-depleted sites. Changes in surface chemical composition and microstructure by electropolishing on corrosion and SCC of Alloy 182 in high-temperature water mitigated the corrosion, intergranular corrosion, and SCC of Alloy 182 [9]. It has also been illustrated that stainless steels experience a sharp growth in pitting corrosion rate as the solution concentration, temperature, or potential was changed marginally [10]. Another study revealed that the austenite phase was less susceptible to pitting corrosion than ferrite [11]. Shibata and Takeyama reported that the pitting potentials of Type 304 and Type 316 stainless steel increase with increasing the amount of chromium in the surface film formed by  $\text{HNO}_3$  treatments [12]. Paula investigated the synthetic urine solution with or without diamond-like carbon (DLC) film under 5 N load and 1 Hz under reciprocating conditions, and the results indicate 60NiTi alloy without thermal treatment, and DLC film has 70 times better corrosion susceptibility [13]. Azarian studied the behavior (erosion–corrosion) of AA5052 aluminum alloy exposed into 3.5 wt% NaCl solution and containing silica sand. It concludes the erosion and corrosion rates happened at an impingement angle of 30° [14]. Jiang Jiaren investigated the effect of dissolved oxygen (0–24 ppm) on erosion–corrosion behavior of En30B alloy under the exposure of 35 wt% silica sand and 3.5% NaCl solution at 30 and 45 °C. It was found the significant effect of temperature on the total erosion–corrosion loss [15]. Suresh studied the corrosion behavior of Al 7075/Al<sub>2</sub>O<sub>3</sub>/SiC MMNCs by dipping the sample for 96 h in hydrochloric acid, sulfuric acid, and 3.5% sodium chloride. The results indicate that the hybrid reveals additional resistance to corrosion [16]. The enhanced density, higher area friction, and bigger size of Al<sub>2</sub>CuMg particles (S-phase) on the rougher surface made it more susceptible to pitting [17]. The surface finish is an important parameter for the corrosion resistance of the surface [18]. In other words, a smoother surface finish reduced the frequency of metastable pitting and it has a greater probability of achieving stable pit growth if the surface was smoother [19]. Realizing the significance of applications of F304 SS steel in chemically exposed environments, present work aims to investigate the effect of ferric chloride solution on its corrosion behavior. Consequently, the effect of chloride solution on forged 304 stainless steel can be illustrated for industrial applications. Moreover, the researcher has clarified the effect

of pitting corrosion, but very fewer have studied on forged 304 stainless steel. Surface degradation due to its exposure to  $\text{FeCl}_3$  solution is studied using SEM and EDX based on standard pitting corrosion test. Morphology and composition of inclusions responsible for accelerating pitting corrosion are identified, and their effect has been discussed in detail. However, the rate of corrosion (CR) is calculated by the equation [20]:

$$\text{CR} = m1 - m2/AT \quad (1)$$

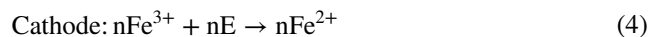
where  $m1$  and  $m2$  are weight losses (mg) earlier and afterward they exposed into test solutions. The  $T$  is a time of exposure (h), and  $A$  is the surface area of the specimens ( $\text{cm}^2$ ).

### 1.1 Rusting Mechanism and Pit Growth

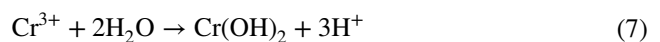
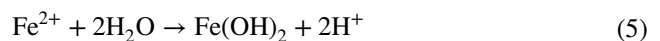
The overall corrosion reaction can be represented by generalized equation:



where  $\text{M}^{n+}$  may be  $n\text{Fe}^{2+}$ ,  $\text{Ni}^{2+}$ , or  $\text{Cr}^{3+}$ . The above equation is the sum of the following half-cell reaction:



where ‘E’ refers to an electron. It is well known that the anodic surface becomes in contact with solutions differing greatly in composition from the initial ferric solution and that these solutions grow relatively concentrated in the chlorides of the reaction products shown in Eq. (1) [21]. A part of the dissolved metal ions further lowers the pH value due to hydrolysis reactions of:



In this situation, the ferric chloride solution ( $\text{FeCl}_3$ ) elements which precipitate from the solution will deposit onto the specimen surface and form a compact  $\text{FeCl}_3$  layer. After the formation of the surface layer, it partially eliminates  $\text{FeCl}_3$  layer which affects the dissolution of the passive film. Since the dissolution rate is not constant over the entire surface, some of the bare metal will be open to the solution prior than the other, which sets up a local anode. Additionally, because of galvanic corrosion, the bare metal part is corroded and it slowly turns into a pit. This galvanic pair forms among the bare metal (works as an anode) and the  $\text{FeCl}_3$  exposed surface (works as a cathode). The remaining metal ions migrate and diffuse outward through the thin water layer, and a part of them lowers the pH value of the

surroundings by hydrolysis reactions (from 4 to 46), leading to an increase in corroded area [16]. Figure 1 depicts a deep growth of pitting corrosion exposed in a chloride environment. It consists of two regions (anode and cathode) as shown. The deep structure of material where pitting is formed is known as an anode region.

These anodic regions are very small as compared to cathode zone produced on the diffused interface which is adequate to electron loss and forms the pitting direction. It was observed that the passive film turns into more critical in nature when it is exposed to the solution of ferric chloride.

## 2 Materials and Methods

Austenite alloys with high chromium weight percent fraction have an inherent capability to protect it from the corrosive environments, and therefore, it takes a number of days or months or maybe years to develop pits on the stainless steel alloy naturally. However, in the current endeavor to examine the effect of corrosion induced by chlorides, experiments were carried out by exposing the material with the help of concentrated chemical solution. Chemical composition of material determined as per ASTM E1086-14 is shown in Table 1.

Five experiments were conducted as per ASTM G-48 standard of procedure A and E, respectively. All specimens considered were of same size, i.e.,  $5.28 \times 2.57 \times 0.31$  cm. These specimens were kept immersed in the  $FeCl_3$  solution of 100 g reagent grade ferric chloride diluted with 900 mL demineralized water. Table 2 shows the configuration of an experiment performed with exposure time and temperature. Morphology and microstructure of the oxide films were investigated on Nova Nano SEM—450 at an accelerating voltage of 10 kV equipped with powerful EDX and Leica optical microscope.

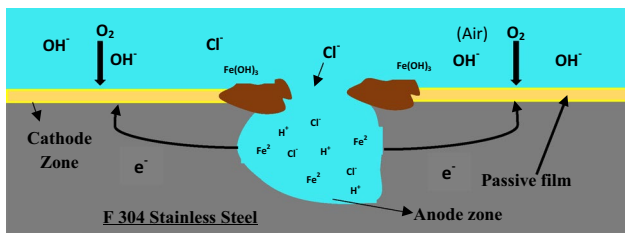


Fig. 1 Deep growth mechanism during pitting corrosion

Table 1 Chemical composition (wt%)

Iron	Carbon	Silicon	Manganese	Phosphorous	Sulfur	Chromium	Nickel	Nitrogen
Balance	0.028	0.361	1.158	0.011	0.001	18.419	8.127	0.10

Table 2 Exposure time and temperature during experiment

Specimen	1	2	3	4	5
Time (h)	08 and 16	24	24	12	24
Temperature (°C)	22	22	50	5	5

## 3 Experimental Results and Discussion

Experiments were carried out on five different specimens kept under a corrosive environment at different temperature and time durations as shown in Table 2. The surface of the specimens was prepared with 220 grit and 420 grit emery paper. During the entire process, eight parameters were investigated as shown in Table 3. After experiments, the specimens were observed under an optical microscope of Leica. The formation of pits is shown in Figs. 2, 3, 4, 5, and 6, respectively.

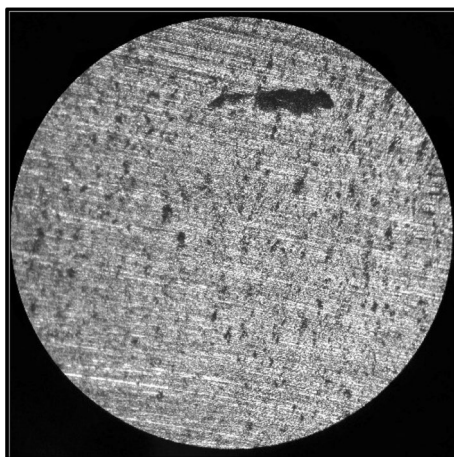
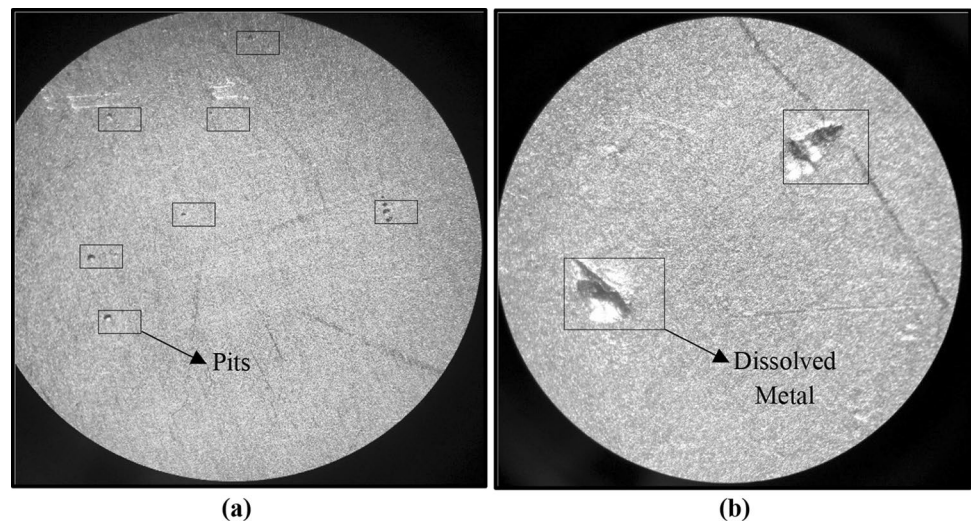
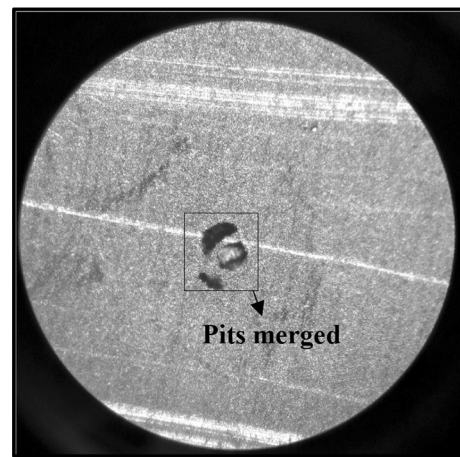
### 3.1 Morphology of Corrosion Attack

The first specimen was put under corrosion test for the duration of 8 h at a temperature of 22 °C. The specimen having a total surface area of 22 (cm<sup>2</sup>) was prepared with 220 grit and 420 grit emery paper. Figure 2a shows the specimen 1 at  $\times 20$  magnification observed under an optical microscope after the exposure of 8 h, and no significant pits have been observed. But the total number of minor pits observed was seventeen. The average pit depth was 0.2410 (mm) as determined with the help of pit depth gauge.

The observed corrosion rate was 0.0011 (g/cm<sup>2</sup>). Specimen 1 is kept under corrosion test for two different time durations of 8 h and 16 h at temperature 22 °C, respectively. Surface morphology was studied at  $\times 20$  magnification using an optical microscope. The average pit depth was measured using a pit depth gauge. Additionally, in a similar way for a different set of experiments were also carried out at different time durations and temperature. During these experimentations, a significant amount of pits has been observed on the surface of the specimen. Moreover, microstructures of all the fine specimens are shown in Figs. 2, 3, 4, 5, and 6 distinctly. Table 3 shows the analysis of the results of all experiments. The result was obtained in combination with the rise of temperature, and the degree of erosion appeared to be more. Hence, the higher temperatures and the start of corrosion will be found higher [22]. For specimen 1 and 2, the corrosion rate increased with increasing the exposure time at room temperature. Moreover, while increasing the degree of temperature solution caused by

**Table 3** Experimental results of five specimens

S. no.	Parameters	Specimen 1		Specimen 2	Specimen 3	Specimen 4	Specimen 5
1	Time duration (h)	8	16	24	24	12	24
2	Temp (°C)	22	22	22	50	5	5
3	Total surface area (cm <sup>2</sup> )	31	31	31	31	31	31
4	Avg. pit depth (mm)	0.2410	0.3610	0.8062	0.9460	0.2	1.3
5	Corrosion rate (g/cm <sup>2</sup> )	0.0011	0.0015	0.0041	0.021	0.0047	0.0054
6	Initial wt. (g)	32.3440	32.3090	30.5530	31.6340	27.3520	29.1010
7	Final wt. (g)	32.3090	32.2600	30.4360	30.9920	27.2190	28.9370
8	Total wt. loss (g)	0.035	0.049	0.117	0.642	0.133	0.164
9	Significant pit observed	No	No	Yes	Yes	No	No

**Fig. 2** Optical image of corroded specimen at 22 °C **a** 8 h and **b** 16 h**Fig. 3** Optical image of corroded specimen at 22 °C, 24 h**Fig. 4** Optical image of corroded specimen at 50 °C, 24 h

intensification in the concentration of the test solution, correspondingly, it also augmented the chemical reaction, thus increasing the solution acidity and corrosion as well.

Figure 7 shows that weight loss of the material is a function of temperature. Contour shows that the weight loss

increases with an increase in exposure time and becomes independent of time duration if kept at a fixed concentration of the solution. For instance, at a temperature of 30 °C for a time duration of 13 h, weight (wt) loss is found to be 0.1 g, but it becomes 0.2 g while the temperature is increased to

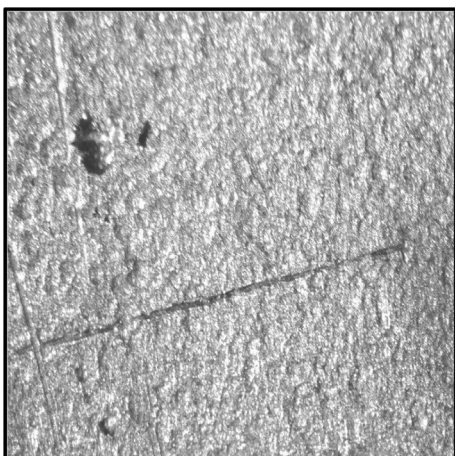


Fig. 5 Optical image of corroded specimen at 5 °C, 12 h



Fig. 6 Optical image of corroded specimen at 5 °C, 24 h

40 °C and still kept for 13 h. Figure 8 shows that average pit depth is a function of both time and temperature. Contours show that average pit depth increases with an increase in both time and temperature.

For instance, at fixed temperature of 20 °C constant horizontal direction shows that pit depth increases with an increase in time, whereas vertical direction shows that pit depth increases with an increase in temperature also. It can be observed from temperature–time–corrosion rate plot in Fig. 9 that resistance to pitting by austenite stainless steel 304 reduces with the increase in corrosion rate, i.e., at lower temperatures (5 °C), corrosion rate is higher in comparison with room temperature (22 °C) and elevated temperatures (50 °C). This signifies the surface of F304 stainless steel dissolves more at low temperature. However, Fig. 9 shows that corrosion rate is a function of temperature only. It is independent of time at fixed temperature for fixed time

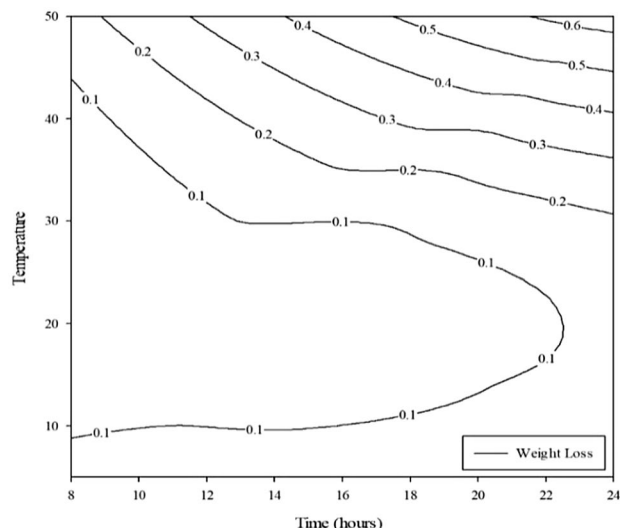


Fig. 7 Weight loss (g) of corroded specimen with respect to time (h) and temperature (°C)

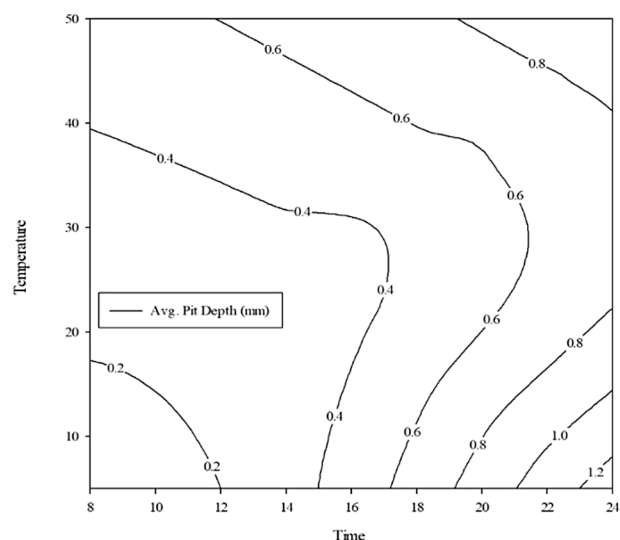
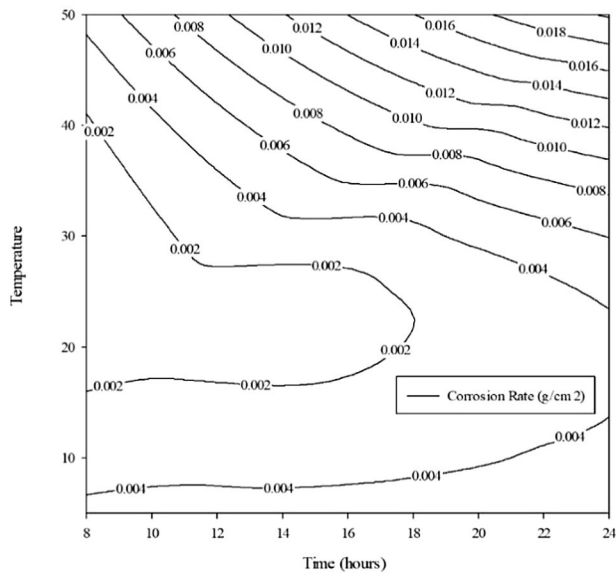


Fig. 8 Avg. pit depth (mm) of corroded specimen with respect to time (h) and temperature (°C)

duration. Similar relation can be seen in Fig. 10 which shows the number of pits increases with an increase in temperature. Contours show that for every fixed time duration, the number of pits increases.

### 3.2 Surface Roughness

Surface roughness parameter profoundly influences the growth of pitting corrosion and pit to crack formation since surface irregularities act as a stress concentration points promoting corrosion phenomenon.



**Fig. 9** Corrosion rate ( $\text{g}/\text{cm}^2$ ) of corroded specimen with respect to time (h) and temperature ( $^{\circ}\text{C}$ )

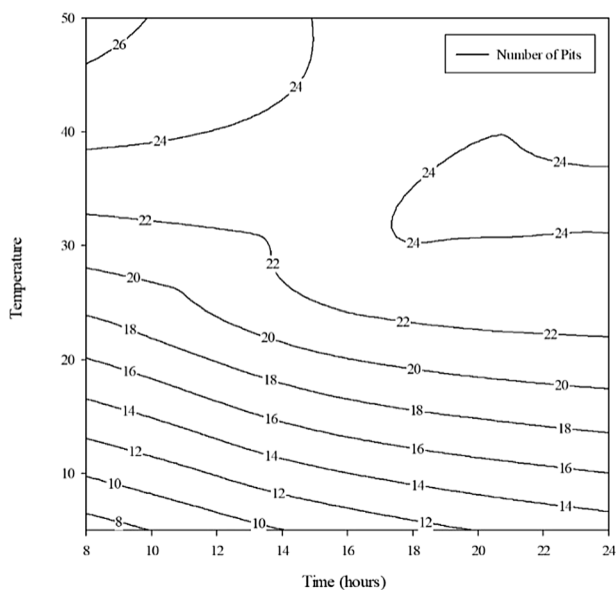


**Fig. 10** No. of pits of corroded specimen with respect to time (h) and temperature ( $^{\circ}\text{C}$ )

However, in spite of its high degree of surface roughness, the smooth surface can be considered as more resistant to the pitting corrosion, because a less number of sites are available for attack. The results show that surface roughness has a strong effect on the initiation of metastable pits shown in Table 4. It has been observed that the surface roughness may affect the number of pit sites. However, extra pit sites may be wide-open if the surface roughness is more and the surface density of the sites is constant [15]. Therefore, lower the temperature, higher is the surface roughness observed. Figure 11a shows the results represent at the centre of the specimen. It was found that at a temperature of  $5^{\circ}\text{C}$  for time duration of 13 h, the surface roughness is measured to  $1.5\ \mu\text{m}$ . Similarly, at temperature of  $13^{\circ}\text{C}$  at time 12.5 h the surface roughness is found to be  $1.0\ \mu\text{m}$ . Further, with an increase in time the surface roughness becomes constant. At  $30^{\circ}\text{C}$ , the surface roughness is almost constant and is found to be  $0.5\ \mu\text{m}$ . Figure 11b illustrates the surface roughness at the edge of the specimen with respect to time and temperature. It was found that the surface roughness becomes constant at temperature of  $30^{\circ}\text{C}$  and above. Surface roughness at edges of the specimen is also reduced with an increase in time.

These series of experiments suggested that the pits start to propagate, and pit to crack transition on rough surface is much easier as compared to smooth surfaces. Moreover, smooth surface affects the less number of sites which further accelerate pit growth.

### 3.3 EDX Analysis

The corroded specimens corresponding to temperature of  $5^{\circ}\text{C}$ ,  $22^{\circ}\text{C}$ , and  $50^{\circ}\text{C}$  kept for an exposure time of 24 h were analyzed using (Energy Dispersive X-Ray) EDX. Equivalent weight percent and atomic percent values as obtained from EDX analysis are given in Table 5 with respective spectra. The ferric chloride inclusion attacks the localized sites and initiates the pit formation. The pit location was identified to find out the varying composition of F304 stainless steel exposed under the ferric chloride solution. Figure 12 shows an EDX analysis of specimen at temperature  $5^{\circ}\text{C}$  and exposure time of 24 h. The results confirm

**Table 4** Results of surface roughness

S. no.	Parameters	Specimen 1	Specimen 2	Specimen 3	Specimen 4	Specimen 5
1	Time duration (h)	16	24	24	12	24
2	Temp ( $^{\circ}\text{C}$ )	22	22	50	5	5
3	Surface roughness (at centre) $R_a$ ( $\mu\text{m}$ )	0.712	0.732	0.758	1.57	2.61
4	Surface roughness (at edge) $R_a$ ( $\mu\text{m}$ )	0.410	0.574	0.586	0.704	3.15

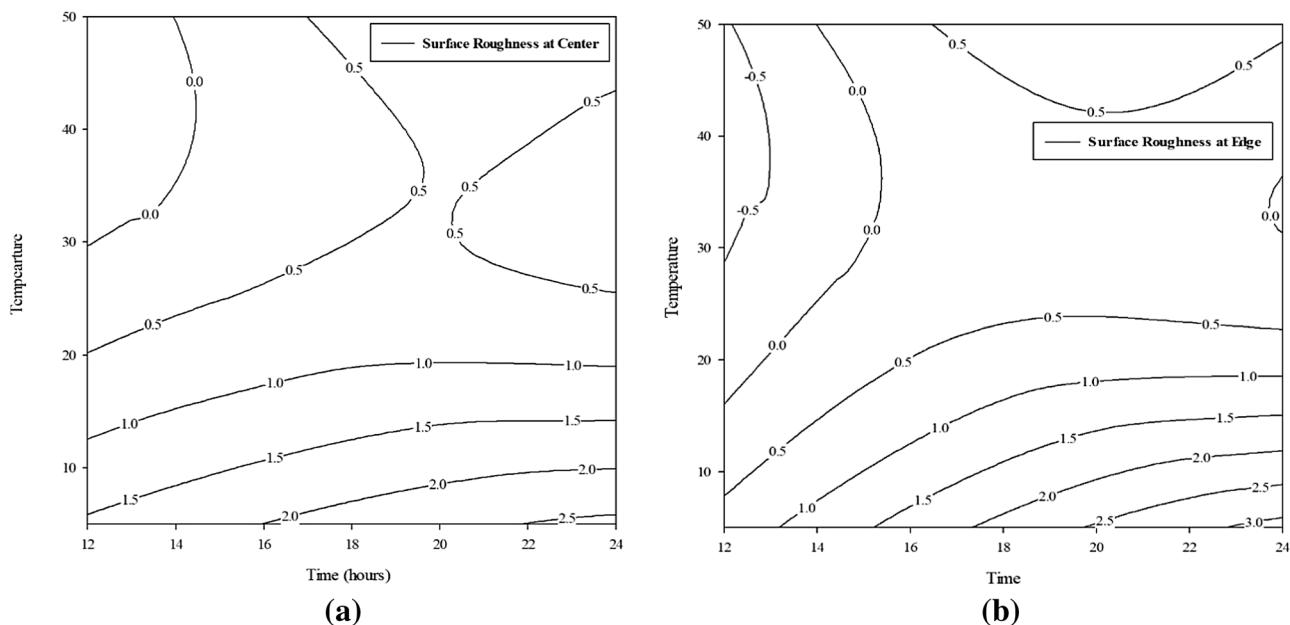


Fig. 11 Surface roughness of F304 stainless steel at a center and b edge

Table 5 Wt% of Cl in all experiments

S. no.	Parameters	Specimen 1	Specimen 2	Specimen 3
1	Temperature (°C)	5	22	50
2	Exposure time	24	24	24
3	wt% of Cl	1.13	0.88	1.65

exposed region as a composition of chloride ion near the pit surface which is 1.13 wt%.

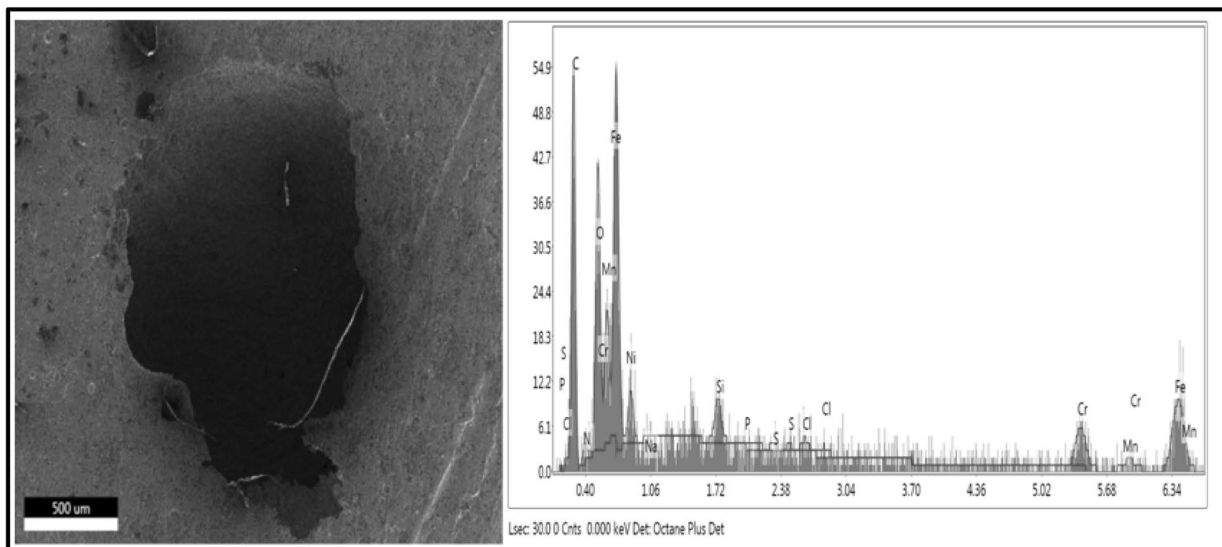
Furthermore, Fig. 13 shows the observed result of EDX analysis of the second specimen exposed in 22 °C for 24 h. Figure 14 represents EDX spectrum of specimen exposure at temperature 50 °C for 24 h. High chloride content has been observed at 50 °C which was 1.65 wt% of total weight wt%. The increased temperature gradually increases the concentration of chloride around the pit surface.

The EDX results reveal that most of the pitting surfaces show a varying chemical composition of the exposed material. The Mn and Cl inclusions were found around the pitting surface, and the plane surface of the material has around 3 wt% of these inclusions. Moreover, oxygen was found around the pitting with 4.52 wt% fraction at room temperature. In corrosive environments, iron oxide is formed when iron and oxygen react in the existence of water/moisture in the air. Chromium which has a highly corrosive resistance shows 22 wt% in the pitting surface. This fraction helps to reform the passive layer around the pitting surface to stop the growth of pits. The result of Fig. 14 confirms that the surface is mostly covered by FeCO<sub>3</sub> and iron oxide.

Table 5 indicates the results of the concentration of chloride wt% on the pitting surface. The oxygen percentage signifies that the air was in contact with metal surfaces and it also augmented the odds of corrosion rate. It is concluded that the chloride concentration increases with an increase in temperature. However, it was observed that corrosion cracking starts at a high concentration of chloride and temperature. Previous studies also specify that the higher temperature is no longer adequate to resist the corrosion in 304 SS. [23]

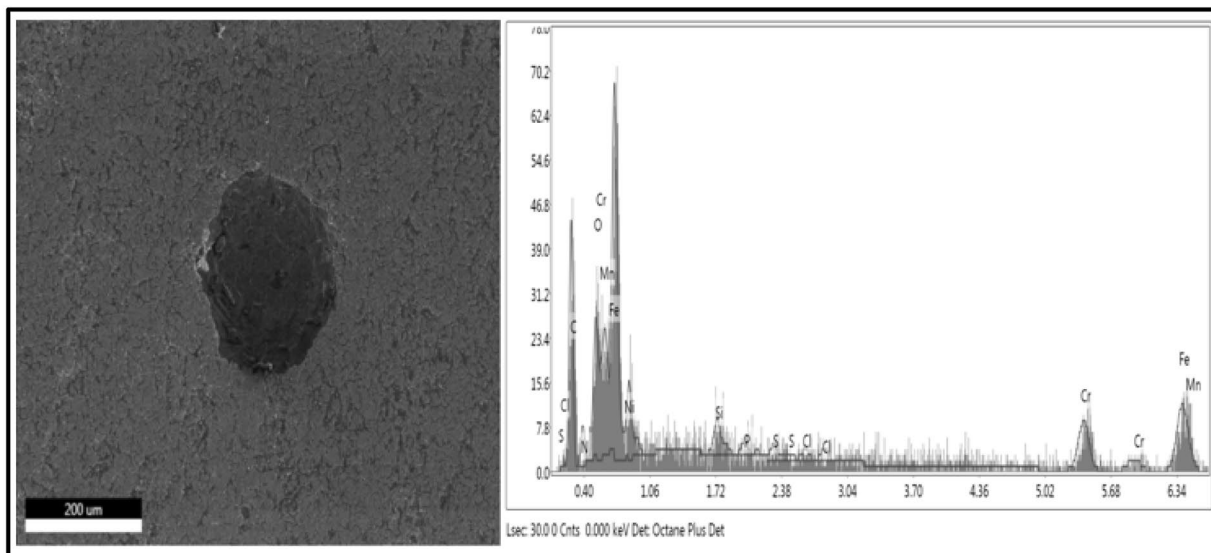
### 3.4 Variation in Corrosion Rate with Mn and Nitrogen

As per the results, Mn and nitrogen were found on the surface of F304 SS and these insertions have a tendency to dissolve into the material and produce a localized attack at the interface of austenite initially. Figure 15a indicates the corrosion rate versus Mn wt%. The Mn wt% was determined with the help of EDX analysis. Specimen “A” represents the specimen exposed to 24 h at 5 °C. Specimen “B” represents the specimen exposed to 24 h at 22 °C, and Specimen “C” represents the specimen exposed to 24 h at 50 °C. Noticeably, materials with maximum temperature of 50 °C show the lowest Mn wt% and the highest corrosion rate. The best resistance to the pitting corrosion in chloride medium showed at room temperature even at the highest Mn wt% inclusion. It was found that the Mn wt% is hardly affected by temperature and start pitting process very fast. Figure 15b reveals nitrogen enrichment at the pitting surface



Elements	C K	N K	O K	Fe L	Ni L	Si K	P K	S K	Cl K	Cr K	Mn K
<b>Weight %</b>	26.91	1.60	8.47	34.07	4.38	1.93	0.38	0.35	1.13	22.85	6.41
<b>Atomic %</b>	60.24	3.07	13.67	16.40	2.00	1.84	0.33	0.29	0.86	11.82	3.14

Fig. 12 EDX image of specimen exposure at temperature 5 °C and time 24 h and the results of EDX analysis of F304 stainless steel



Elements	C K	N K	O K	Fe L	Ni L	Si K	P K	S K	Cl K	Cr K	Mn K
<b>Weight %</b>	16.75	3.73	4.52	31.29	5.45	1.55	0.95	0.90	0.88	27.03	6.95
<b>Atomic %</b>	41.24	7.87	<b>8.36</b>	<b>16.57</b>	2.75	1.63	0.91	0.83	0.74	15.37	3.74

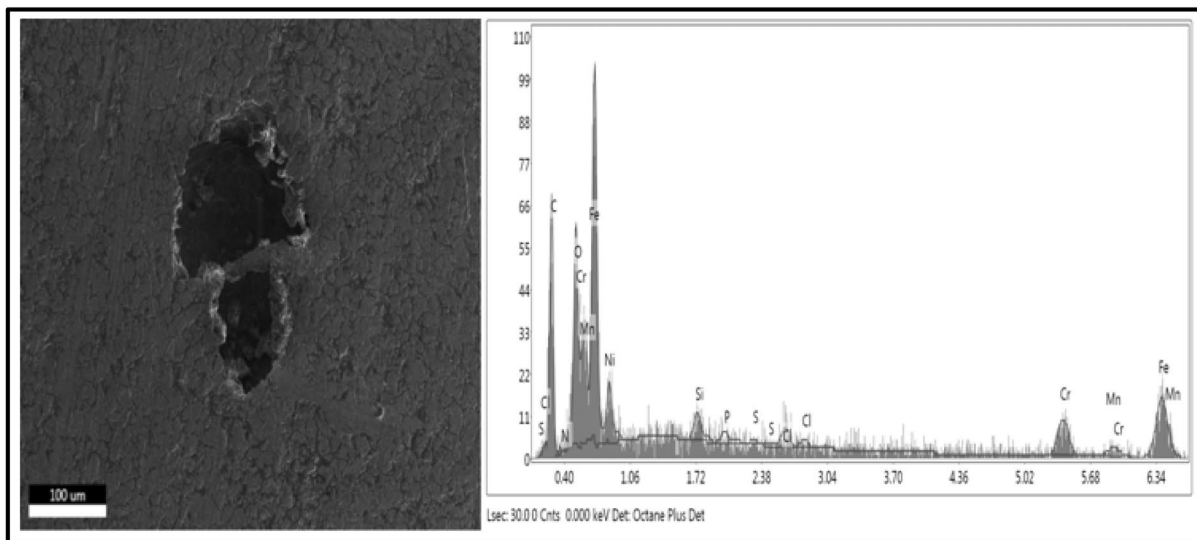
Fig. 13 EDX image of specimen exposure at temperature 22 °C and time 24 h and the results of EDX analysis of F304 stainless steel

interface as compared to without pitting surface. This nitrogen enrichment increases with an increase in temperature

leading to nitrite formation. The dissolution reaction of electrochemical nitrogen can be signified as:







Elements	C K	N K	O K	Fe L	Ni L	Si K	P K	S K	Cl K	Cr K	Mn K
Weight %	18.86	1.43	6.89	37.32	4.95	1.24	0.71	0.38	1.65	21.36	5.21
Atomic %	45.04	2.93	12.34	19.17	2.42	1.27	0.66	0.34	1.34	11.78	2.72

Fig. 14 EDX analysis of F304 stainless steel of specimen exposed at temperature 50 °C for 24 h

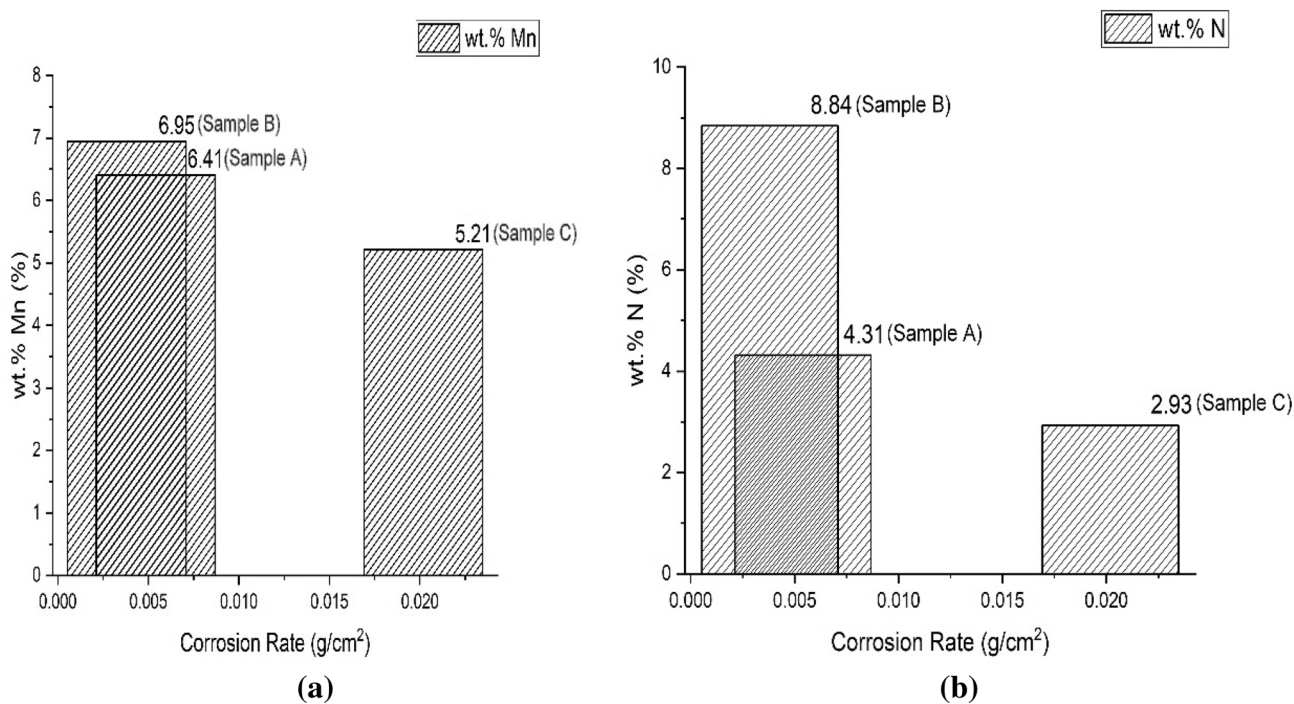


Fig. 15 Variation in the corrosion rate as a function of a Mn and b nitrogen at pit surface

### 3.5 SEM Analysis

The pit surface morphologies of corroded specimens at different magnifications have been observed. Figure 16a depicts

the surface of the F304 stainless steel alloy exposed under 12 h at 5 °C. It was found that in Fig. 16a, the surface of the exposed steel becomes brittle which helps to develop a tiny amount of cracks/pits throughout the surface. Figure 16b



Fig. 16 SEM images of F 304 stainless steel at 5 °C and exposed under 12 h

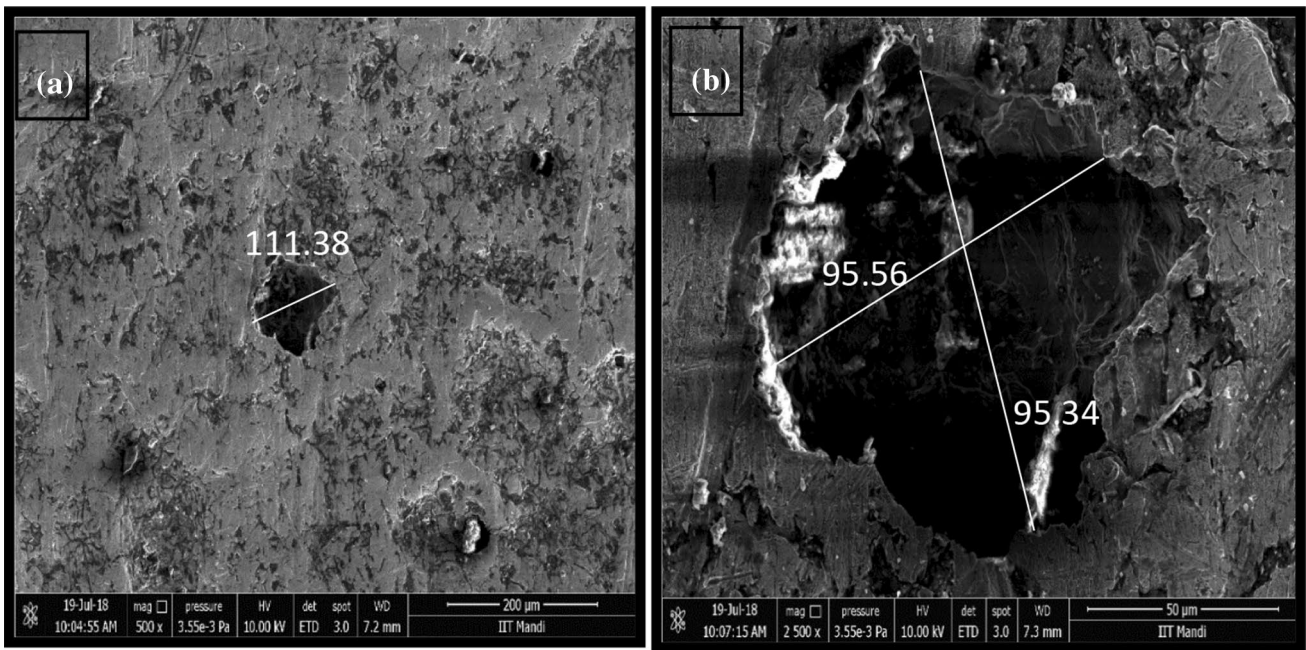


Fig. 17 SEM morphology of stainless steel alloy exposed at 5 °C under 24 h

shows the hemispherical pit size being developed on the surface of alloy. The pit bottom has large opened surface. As shown in Fig. 16b, a small number of cracks and crack-like topographies can be seen nearby the pit boundary. Figure 17 reveals the surface morphology of the alloy exposed in chemical solution at the temperature of 5 °C and time 24 h

which (a) expressed the surface of the corroded alloy and (b) represented the hemispherical pit geometry. The distance of 95.56 μm and 95.34 μm was calculated by using software “Imagej”.

It was found that the surface of alloy revealed many tiny cracks throughout the surface which will further initiate

the localized crack and then start to propagate. Figure 18c shows the small cracks at the pit bottom site, and it was most likely to crack easily. The small amount of inclusion was found at the bit bottom which will act as an electrolyte and increase material degradation. Figure 19a shows the pit geometry of hemispherical type and (b) represents inclusion at the surface of pit bottom. In most of the cases,

this inclusion also helps to initiate the more pit at the surface of pit bottom. Further, SEM image also revealed that the corrosion cracking has initiated from the pit base and from the intergranular corroded area. The surface texture of the exposed specimens formed corrosion layer after 12 h (at 5 °C), 24 h (at 5 °C), 16 h (at 22 °C), and 24 h (at 22 °C), respectively. Figure 18a shows the corrosion

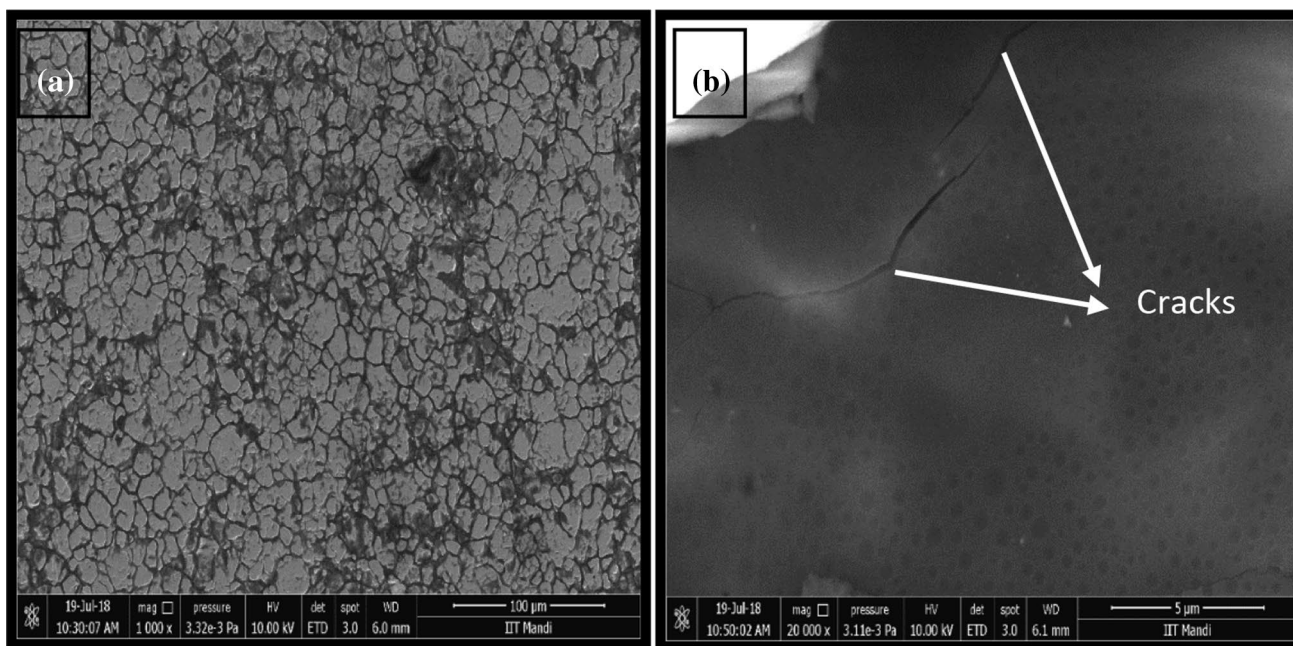


Fig. 18 SEM image of alloy exposed at the temperature of 22 °C and 16 h

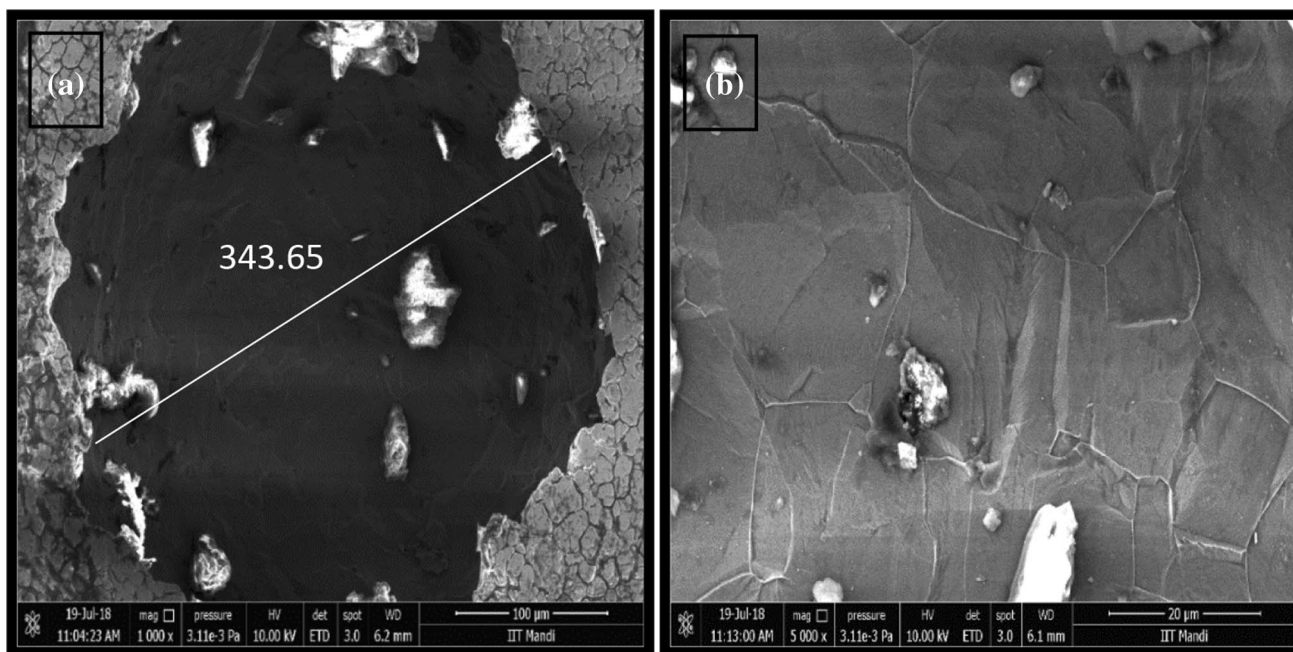
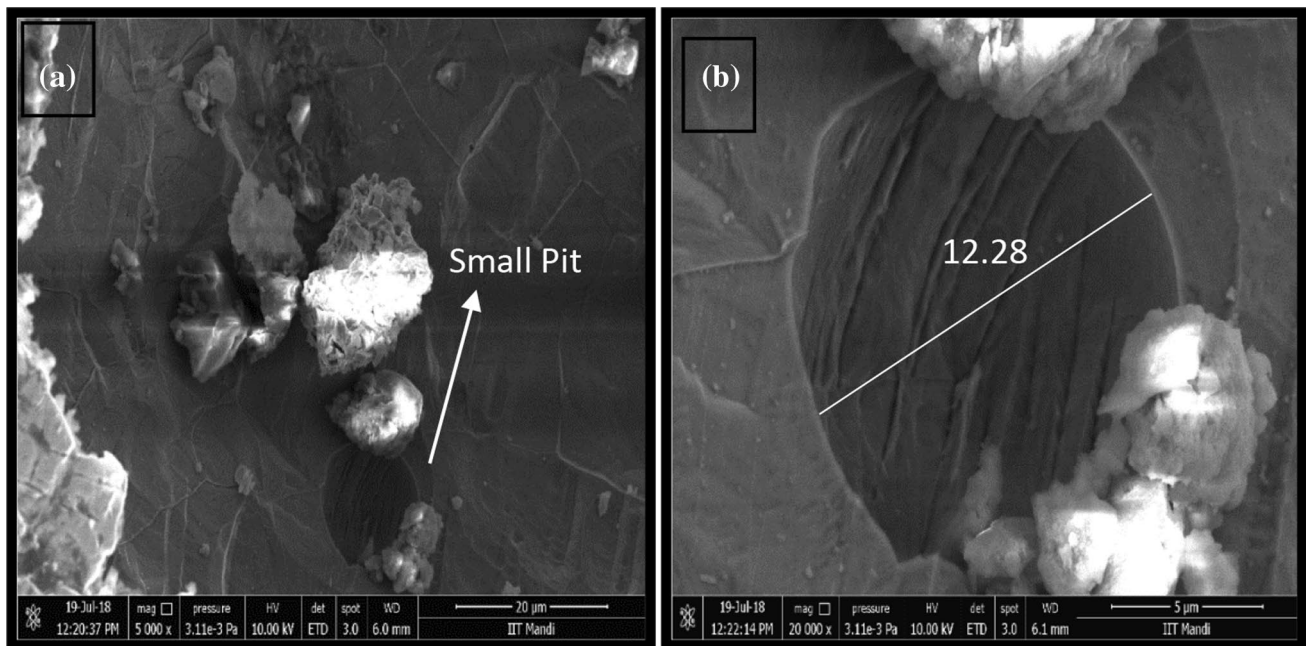


Fig. 19 SEM images of alloy exposed at a temperature of 22 °C and 24 h



**Fig. 20** SEM images of alloy exposed at the temperature 50 °C and 24 h

layer, which had many cracks on the entire surface possibly will be the corrosion layer in progress to develop, and it takes place from altered spots on the surface and creates many “landmasses” of corrosion product. Once these “land mass” produced and overlapped with together, deep cracks were developed among them. Moreover, it was determined that as the specimen corroded, the chemical solution in which specimen exposed slowly reached saturation. Primarily, the  $\text{FeCl}_3$  deposit on the surface of the specimen and overlies the cracks. The corrosion layer turns into shielding and accordingly the corrosion rate reduced. Figure 20a represents the small pits at the bottom of the pit. Furthermore, in view of this, characterization of steels with high-end microscopy advanced techniques is essential [24–27].

Usually, the material degradation was more inside the pitting surface. Therefore, the internal surface of pit is more corrosive in nature and the pit tries to meet together through inside the pitting surface. Figure 20b also represents that the pit was trying to damage the material from inside the alloy. It has been revealed that Mn has a strong attraction to sulfur to proceed extremely stable MnS inclusions and, as a consequence, it typically seems to proceed these sulfides within austenite stainless steel microstructure. Stainless steel assessed here confirms the existence of manganese sulfide inclusions which allows revealing the different mechanism of Mn action with respect to corrosion rate.

Under the acidic environments, Mn was speedily dissolved and let the creation of excessive amount of oxidized above the pitting surface, which let the re-passivation process. The chemical solution found more aggressive at high temperature under the investigated environments.

## 4 Conclusion

Based on the extensive experimentation carried out on F304 stainless steel alloy being subjected to pitting corrosion tests for varying time and temperatures (5 °C, 22 °C, and 50 °C), The following conclusions are obtained:

1. An increase in time period leads to an increment in the number of pits, whereas an increase in temperature (up to 50 °C), the corrosion rate decreases. This leads to the conclusion that proper attention should be taken while using F304 stainless steel during operations at high and low temperature.
2. EDX analysis revealed the dissolution of chloride in abundance around the pitting surface which appears to be responsible for pits formation and inclusion.
3. Observations on pit morphology with light microscopy showed pitting probability and pit average size and depth of pits. It was found that surface finish shows a significant role in the corrosion behavior, but this connection was found to be not as expressively when a chloride-containing solution was used. A possible reason for this

behavior should be fierceness of the chloride ions in the direction of the stainless steel's passive layers.

4. The corrosion rate increases with pit depth, and material weight loss increases with an increase in temperature. It was also found that the chloride concentration was more aggressive at low temperature as compared to room temperature.
5. It is also understood that small cracks and tiny pits more easily start to initiate at the pit bottom surface and more corrosive in nature as compared to the top surface of the specimen. Furthermore, material degradation was faster at the pit bottom, and it is more susceptible for the generation of new pits and cracks.

## Compliance with Ethical Standards

**Conflict of interest** On behalf of all authors, the corresponding author states that there is no conflict of interest.

## References

1. Vogiatzis CA, Kountouras DT, Skolianos SM (2016) Corrosion behavior of 304 stainless steel in simulated oilfield produced water. *Corros Eng Sci Technol* 51(1):51–59
2. Street SR, Mi N, Cook AJ, Mohammed-Ali HB, Guo L, Rayment T, Davenport AJ (2015) Atmospheric pitting corrosion of 304L stainless steel: the role of highly concentrated chloride solutions. *Faraday Discuss* 180:251–265
3. Degerbeck J, Karlsson A, Berglund G (1979) Atmospheric corrosion of stainless steel of type 18Cr–2Mo–Ti. *Br Corros J* 14(4):220–222
4. Degerbeck J, Karlsson A, Berglund G (1979) Atmospheric corrosion of stainless steel of type 18Cr–2Mo–Ti. *Br Corros J* 14(4):220–222
5. Ghosh S, Kain V (2010) Microstructural changes in AISI 304L stainless steel due to surface machining: effect on its susceptibility to chloride stress corrosion cracking. *J Nucl Mater* 403(1):62–67
6. Xie Y, Guo S, Leong A, Zhang J, Zhu Y (2017) Corrosion behaviour of stainless steel exposed to highly concentrated chloride solutions. *Corros Eng Sci Technol* 52(4):283–293
7. Prosek T, Iversen A, Taxén C, Thierry D (2009) Low-temperature stress corrosion cracking of stainless steels in the atmosphere in the presence of chloride deposits. *Corrosion* 65(2):105–117
8. Prosek T, Le Gac A, Thierry D, Le Manchet S, Lojewski C, Fanica A et al (2014) Low-temperature stress corrosion cracking of austenitic and duplex stainless steels under chloride deposits. *Corrosion* 70(10):1052–1063
9. Han Y, Han EH, Peng Q, Ke W (2017) Effects of electropolishing on corrosion and stress corrosion cracking of Alloy 182 in high temperature water. *Corros Sci* 121:1–10
10. Punckt C, Bölscher M, Rotermund HH, Mikhailov AS, Organ L, Budiansky N et al (2004) Sudden onset of pitting corrosion on stainless steel as a critical phenomenon. *Science* 305(5687):1133–1136
11. Huang TS, Tsai WT, Pan SJ, Chang KC (2018) Pitting corrosion behaviour of 2101 duplex stainless steel in chloride solutions. *Corros Eng, Sci Technol* 53(sup1):9–15
12. Hong T, Ogushi T, Nagumo M (1996) The effect of chromium enrichment in the film formed by surface treatments on the corrosion resistance of type 430 stainless steel. *Corros Sci* 38(6):881–888
13. Paula LO, Sene AC, Manfroi LA, Vieira AA, Ramos MAR, Fukumasu NK et al (2018) Tribo-corrosion and corrosion behaviour of titanium alloys with and without DLC films immersed in synthetic urine. *J Bio Tribo Corros* 4(3):51
14. Azarian NS, Ghasemi HM, Monshi MR (2015) Synergistic erosion and corrosion behavior of AA5052 aluminum alloy in 3.5 wt% NaCl solution under various impingement angles. *J Bio Tribo Corros* 1(2):10
15. Jiang J, Xie Y, Islam MA, Stack MM (2017) The effect of dissolved oxygen in slurry on erosion–corrosion of En30B steel. *J Bio Tribo Corros* 3(4):45
16. Suresh S, Gowd GH, Devakumar MLS (2018) Corrosion behaviour of Al 7075/Al 2 O 3/SiC MMNCs by weight loss method. *J Bio Tribo Corros* 4(4):62
17. Tian W, Chao B, Xiong X, Li Z (2018) Effect of surface roughness on pitting corrosion of 2A12 aluminum alloy. *Int J Electro Chem Sci* 13(3):3107–3123
18. Hilbert LR, Bagge-Ravn D, Kold J, Gram L (2003) Influence of surface roughness of stainless steel on microbial adhesion and corrosion resistance. *Int Bio Deterior Biodegrad* 52(3):175–185
19. Burstein GT, Pistorius PC (1995) Surface roughness and the metastable pitting of stainless steel in chloride solutions. *Corrosion* 51(5):380–385
20. Tsutsumi Y, Nishikata A, Tsuru T (2007) Pitting corrosion mechanism of Type 304 stainless steel under a droplet of chloride solutions. *Corros Sci* 49(3):1394–1407
21. Sherif E-SM (2011) Corrosion behavior of duplex stainless steel alloy cathodically modified with minor ruthenium additions in concentrated sulfuric acid solutions. *Int J Electrochem Sci* 6:2284–2298
22. Arwati IA, Majlan EH, Daud WRW, Shyuan LK, Arifin KB, Husaini T et al (2018) Temperature effects on stainless steel 316L corrosion in the environment of sulphuric acid (H<sub>2</sub>SO<sub>4</sub>). *IOP Conf Ser* 343(1):012016
23. Ahmed SR (2016) Influence of high temperature on corrosion behavior of 304 stainless steel in chloride solutions. *AIP Adv* 6(11):115301
24. Akhtar M, Khajuria A, Kumar R, Bedi R (2017) Metallurgical Investigations on dual heat cycled boron alloyed P91 ferritic/martensitic steel. In: *Proceedings of Young Professionals International Conference*, p C080
25. Khajuria A, Modassir Akhtar D, Kumar R, Jaganathan Swaminathan D, Bedi R, Shukla DK (2010) Effect of boron modified microstructure on impression creep behaviour of simulated multi-pass heat affected zone of P91 steel. Dr. Samik Dutta Dr. Shitan-shu Shekhar Chakraborty, 150
26. Akhtar M, Khajuria A, Sahu JK, Swaminathan J, Kumar R, Bedi R, Albert SK (2018) Phase transformations and numerical modelling in simulated HAZ of nanostructured P91B steel for high temperature applications. *Appl Nanosci* 8(7):1669–1685
27. Khajuria A, Bedi R, Kumar R (2019) Investigation of impression creep deformation behavior of boron-modified P91 steel by high-end characterization techniques. *Manufacturing Engineering*. Springer, Singapore, pp 137–150

**Publisher's Note** Springer Nature remains neutral with regard to jurisdictional claims in published maps and institutional affiliations.